7

Intravascular magnetic resonance imaging (MRI)

V. ACIKEL and E. ATALAR, Bilkent University, Turkey

DOI: 10.1533/9780857097477.2.186

Abstract: This chapter discusses the advantages of using MRI in intravascular operations. Beginning with a brief explanation of some sample intravascular MR operations, the chapter goes on to outline the visualization problem of catheters under MRI. Some of the fundamental catheter coil designs are shown and a range of imaging techniques for catheter tracking are discussed. Finally, safety issues related both specifically to these catheter coil designs and to MRI more generally are explored.

Key words: MRI interventions, intravascular MRI procedures, MR catheter loop coils, MR catheter safety.

7.1 Introduction

The use of X-ray fluoroscopy in guiding vascular interventional procedures has been in clinical practice since the late 1920s and is still successfully implemented today. X-ray fluoroscopy is capable of providing information about interventional devices such as catheters and guidewires. However, its ability to provide information about the soft tissue is limited. MRI, which produces images with a high soft-tissue contrast, is therefore an important alternative to X-ray guidance of interventional procedures. In order to fully utilize the capabilities of MRI in these procedures, both 2D and 3D methods can be employed to register the previously obtained MR images onto the X-ray fluoroscopic images.[1] However, these methods complicate the execution of the procedure and imperfections of the registration process can decrease the utility of MRI. More importantly, use of these techniques may prevent online determination of the success of the procedures from being conducted. As an example, if MRI, rather than X-ray, is used to guide a balloon angioplasty procedure, it will be possible to analyze plaque composition and morphology both before and after the procedure.

Supported by the availability of wide bore and short magnets, MRI has become a good candidate for guidance in intravascular operations. MRI guidance can be conducted without the use of contrast agents, which is critically important for patients with kidney failure, whilst the fact that it does not use ionized radiation means that the procedure can be used in

children and pregnant women without putting them at risk from the harmful effects of X-ray exposure. MRI can also be used to evaluate blood vessel diseases, as electrocardiographically (ECG) gated imaging and segmented k-space GRE sequences provide fast and high-resolution images of vessels and allow imaging of the heart at many cardiac phases.[2]

However, there are also a number of problems related to the use of MRI during intravascular operations. Although MRI provides high tissue contrast, interventional devices such as catheters and guidewires are difficult to visualize since these devices produce no MRI signal; they are visible only as signal void in the images. Traditional catheters must therefore be modified in order to make them visible under MRI. However, the interaction of interventional devices with high static magnetic and strong radio-frequency (RF) electromagnetic fields must be considered when attempting to solve this problem. The first reason for this is that a very high static magnetic field applies strong forces on ferromagnetic materials; a problem which can easily be solved by using non-ferromagnetic materials in the design of the interventional devices. The second key reason is that the coupling of RF fields to the interventional devices can cause severe tissue burns at their tip.

Although the use of MRI intravascular procedures is still a developing area, the advantages mentioned above make it a good candidate for guiding many minimally invasive cardiovascular operations, such as treatment of atrial fibrillation, aortic valve replacement, transvascular access to mesenteric vein system and balloon angioplasty operations.

In this chapter, brief explanations of some sample intravascular MR procedures are described and interventional device visualization techniques are explained. The MRI procedures discussed are chosen such that MRI can improve the success rate of the treatment. Following an introduction to MRI intravascular operations, the technical aspects of active and passive catheter tracking methods using catheter coils are discussed and the SNR performance of catheter coils is explained. Finally, safety aspects of the MRI catheters and the associated required testing are explored.

7.2 Intravascular magnetic resonance (MR) operations

Conventional X-ray angiography techniques are capable of imaging interventional devices in real-time. They are also able to provide information about the chambers of the heart and vessel lumen, via the use of contrast agents. However more in-depth information about the cardiovascular system, such as vessel-wall morphology, is beneficial for more accurate intravascular operations. A sample set of these operations, including cardiac

ablation for atrial fibrillation, aortic valve replacement, transvascular access to mesenteric venous system, recanalization of chronic total occlusion, diagnostic intravascular imaging of atherosclerotic plaques and balloon angioplasty operations under MRI, will now be discussed.

7.2.1 Intravascular imaging of atherosclerotic plaques

Although magnetic resonance imaging of atherosclerotic plaques is currently carried out using surface coils,[3,4] the image resolution is not sufficient for showing deep structures such as coronary arteries.[5] This problem can be overcome by using catheter coils, which improve SNR and produce better quality, higher resolution images. However, it is hard to compare the efficiency of catheter coils as results vary according to the conditions in which the coils are used, as will be discussed further later in this chapter. For more detailed information regarding the performance analysis of coils, see references 7 and 8.

With current advances in catheter coil designs, high resolution MR images of blood vessel walls can be obtained, and by using catheter coils[9–11] not only is it possible to measure the size and the shape of plaques (Fig. 7.1) but also, by using T2 weighted images, the plaque composition (Fig. 7.2).[9]

Rogers *et al.*[12] and Zimmermann-Paul *et al.*[13] also showed that high resolution imaging is possible with an intravascular coil placed on a balloon catheter, and human renal arteries are imaged used this technique.[14] Imaging coronary artery plaques using intravascular MRI on people has also been shown to be feasible, although currently challenging.[15] These feasibility studies demonstrate that intravascular MRI can be safely used in people. The challenge now is to determine the utility and cost-effectiveness of this technique by further studies.

7.2.2 Stent visualizations

With the development of fast imaging techniques, MR has the potential to provide noninvasive assessment of the vascular system. However, in the case of assessment of stent patency, conventional MR techniques are not successful due to material-dependent susceptibility artifacts. Quick *et al.*[16] showed that designing stents as RF antennas means they can be used as RF signal amplifiers. This enables long-term assessment of the stent. In Fig. 7.3, different stent designs in the form of inductively-coupled RF antennas and their signal amplification inside the uniform phantom are shown. Spuentrup *et al.*[17] demonstrate stent placement under MRI guidance, by placing 10 out of 11 stents correctly using this technique. Replacement of the stent is shown in Fig. 7.4.

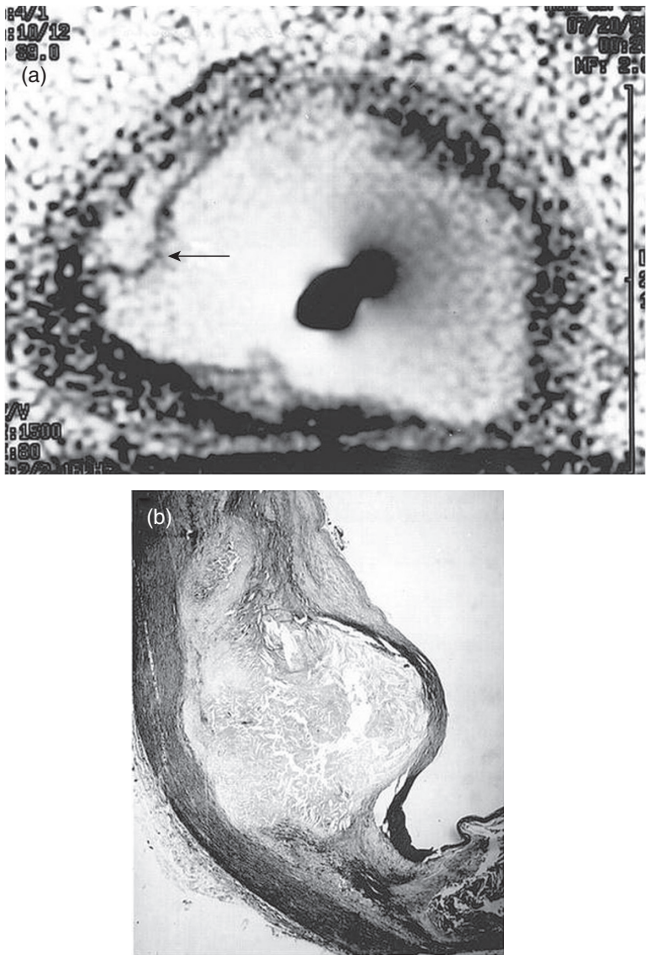

7.1 Axial T2-weighted IVMRI image of aortic cross-section with atherosclerotic plaque (a, arrow). The IVMRI image shows a dark region on top of the plaque, which corresponds to the fibrous cap shown by histopathology (b, Masson stain). The region inside the plaque, the necrotic core, is bright by IVMRI. Republished from Reference 11.

7.2.3 MR-guided recanalization of chronic total occlusion

While chronic total occlusion (CTO) can be visualized under X-ray, determining the position of the occluded portion of the vessel is not possible. The minimally invasive recanalization procedure under X-ray therefore requires an experienced interventionalist and has a high failure rate.[18] However, it is estimated that with the high soft-tissue resolution of MRI, recanalization of CTO can be conducted with a high success rate and

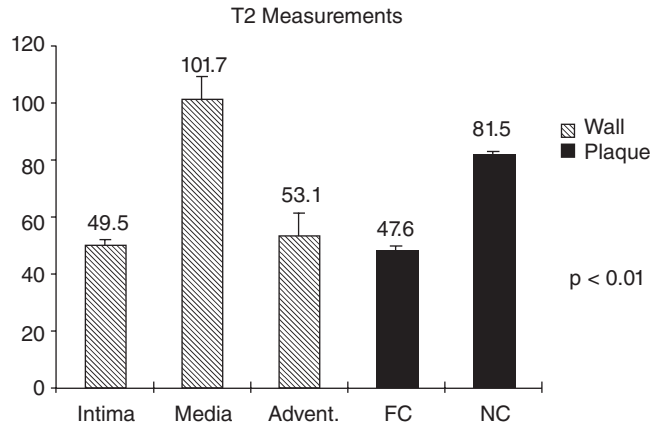

7.2 Means ± SEs of T2 measurements from atherosclerotic plaque and arterial wall components. Thickened intima, fibrous cap (FC), and aortic adventitia have low T2 values, while the necrotic core (NC) and aortic media appear bright in T2-weighted images because of their high T2 relaxation times. The *P* value refers to the overall difference obtained by one-way analysis of variance. Republished from Reference 11.

eventually become a low failure risk procedure. Raval *et al.*[18] showed CTO recanalization in pig models. Custom-made MRI catheters were used with real time MRI for the CTO recanalization, and it was successfully performed in 11 pigs out of 14.

7.2.4 MR-guided treatment of atrial fibrillation

Atrial fibrillation is the most common cardiac arrhythmia. In a healthy heart, the impulse generated by the sinoatrial (SA) node is propagated to the atrioventricular (AV) node by the intermodal pathways in the atrial walls. However, in the case of abnormalities in the conduction pathway between the SA node and AV node, there will be fibrillation in atrial activity. These abnormalities can be treated by surgical ablation or catheter ablation.[19] Catheter ablation operations are currently conducted under X-ray fluoroscopy, as X-ray imaging offers high frame-rates and high resolution, facilitating visualization of the catheter. The use of X-ray does, however, expose the patient and the physician to ionized radiation. Furthermore, due to the X-rays' limited capability of imaging soft tissue, it is not possible to determine the position of the catheter inside the heart[20] and the success of the ablation cannot be tracked. However, using developing MRI techniques, both visualization of the catheter inside the heart[20] and monitoring of the thermal ablation[21] are possible. In work conducted by Susil *et al.*[20] an electrophysiology (EP) MRI catheter is proposed and a diagram of the

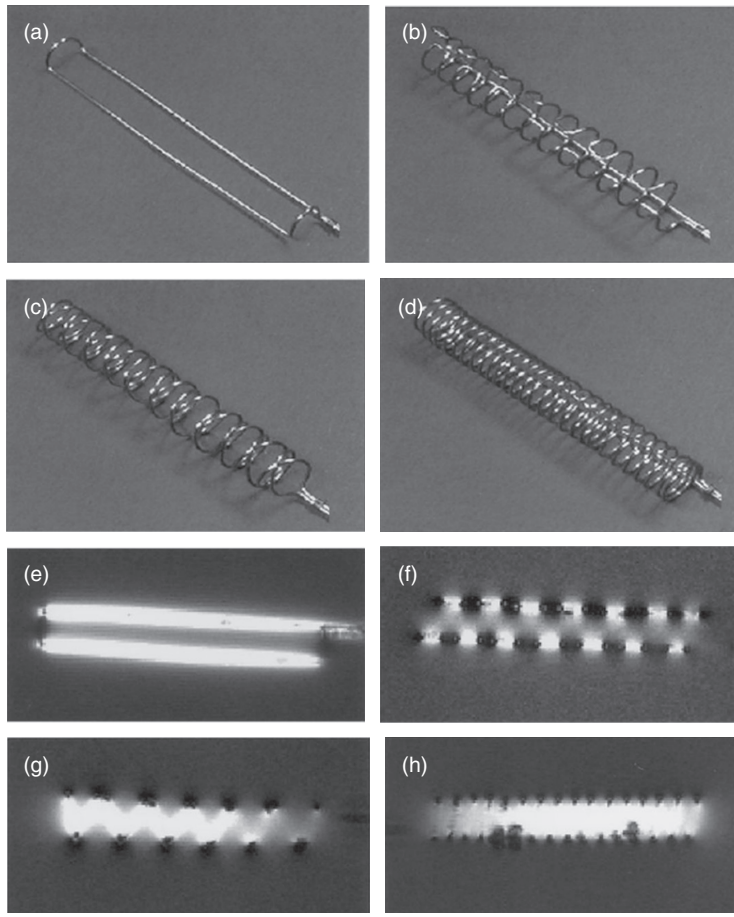

7.3 (a–d) Self-resonant stent prototypes constructed from copper wire, and (e–h) the corresponding signal characteristics in high-resolution MR images. Stent designs from left to right: (a) single-loop, (b) Gianturco, (c) helix, and (d) solenoid. For imaging, the stents were immersed in a NaCl phantom. The body coil served as a transmitter, and a loop surface coil around the phantom served as an RF receiver that inductively coupled to the stent prototypes. A 2D FLASH sequence with small flip angle was employed for image acquisition (e–h) (TR/TE 200/11 ms, FOV 100 × 100 mm, matrix 256 × 256, slice 2 mm, flip 5°, time 54 s). A 70 × 35 mm image portion is shown. Note that the solenoidal design (d) provided the highest signal homogeneity (h) inside the stent lumen. The signal drop-outs (h) inside the solenoidal design are due to excess dip coating. Republished from Reference 16.

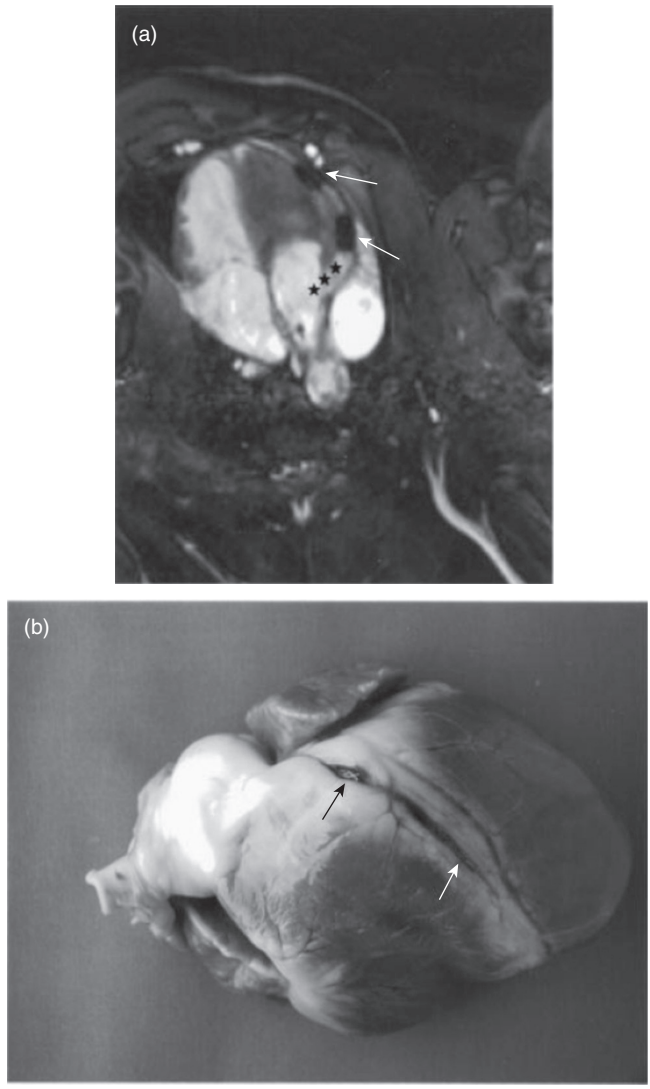

7.4 Double-oblique fast 3D SSFP coronary MRA scan in parallel to the left coronary artery after MR-guided placement of two stainless steel stents in the left coronary artery (a, arrows). Stars indicate left ostium. At autopsy, stent location (b, arrows) was consistent with coronary MRA data. Republished from Reference 17.

physical and electrical structure of such a EP/MRI catheter is shown in Fig. 7.5. Susil *et al.* demonstrate a two-wire EP catheter that can simultaneously record the intracardiacelectrogram (IEGM) and the MR signal, using a loop catheter antenna to receive the MR signal and two electrodes to record the EP signals. These two electrodes can also be used for ablation of the tissue.

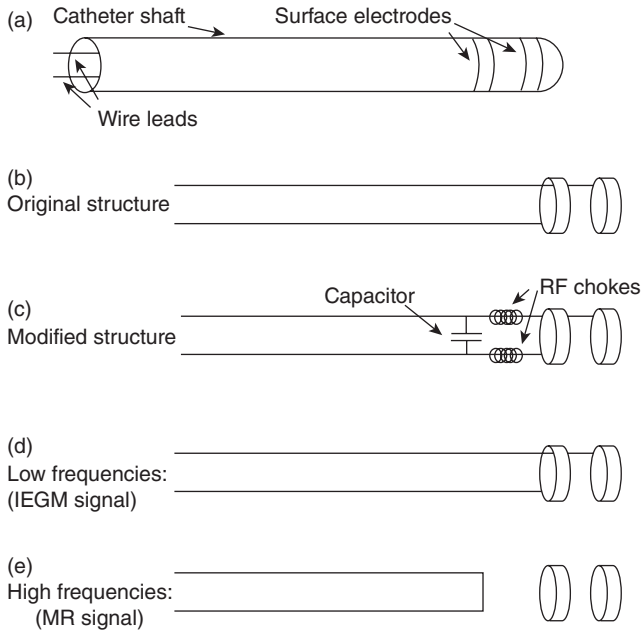

7.5 (a) Physical structure of a standard electrophysiology (EP) catheter. (b) Unmodified electrical structure of the EP catheter. (c) Modified catheter structure. (d) Low-frequency topology of the modified catheter. Note that the low-frequency structure, which is for intracardiac electrogram (IEGM) recording, is identical to the unmodified catheter structure. (e) High-frequency topology of the modified catheter (a loop receiver with surface electrodes decoupled). Republished from Reference 20.

Application of the proposed catheter is demonstrated in Plate XX (see colour section between pages 182 and 183), where tracking of the catheter is shown, with movement of the catheter explained step-by-step and the recorded EP signal shown for each position. Nazarian *et al.* also developed an EP catheter and used this in two patients,[22] having first proved the safety of the catheters in animal experiments. After standard fluoroscopy-guided ablation to address typical atrial flutter, patients were moved to an MR scanner and EP catheters were positioned. The positioning of the catheters was then checked using intracardiac electrogram recordings.

Characterization of lesions is also possible with MRI. Dickfeld *et al.*[23] created lesions on the epicardium using different power levels. After injection of gadolinium, T1-weighted fast gradient echo images were obtained several times during the 10-hour period following the ablation. Four distinct signal enhancements were observed. In Fig. 7.6, MR images obtained at different time points after injection of the gadolinium are

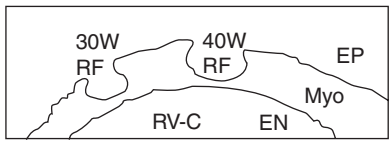

(a) Schematic of anatomic orientation in MR images

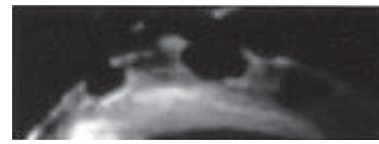

(b) Phase 1: Contrast void (1 min)

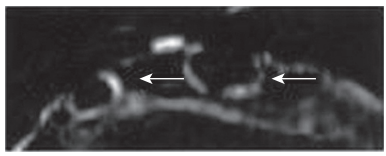

(c) Phase 2: Peripheral enhancement I (15 min)

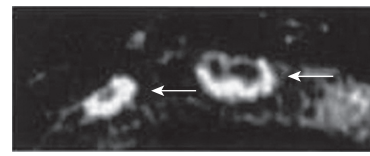

(d) Phase 2: Peripheral enhancement II (45 min)

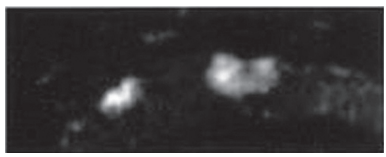

(e) Phase 3: 'Very' delayed enhancement (85 min)

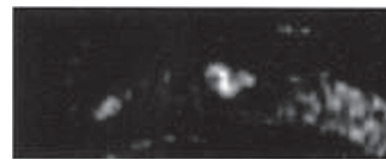

(f) Phase 4: Loss of enhancement (600 min)

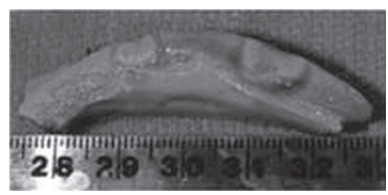

(g) Pathological specimen

7.6 Gadolinium enhancement of a radiofrequency ablation lesion. The time-course (1 to 600 min) after injection of 0.225 mmol/kg gadolinium demonstrates four characteristic phases of enhancement: (a) Schematic of magnetic resonance (MR) images (30-W radiofrequency [RF] and 40-W RF = 30- and 40-W RF ablation lesions; Myo = right ventricular myocardial wall; EP = epicardial side; EN = endocardial side; RV-C = right ventricular cavity). (b) Phase 1 with a contrast void. (c and d) Phase 2 displaying an increasing peripheral enhancement (white arrows). (e) Phase 3 showing 'very' delayed enhancement with high signal intensity throughout the ablation lesion. (f) Phase 4 displaying loss of enhancement with decreasing signal intensity and lesion size. (g) Corresponding pathological specimen. Republished from Reference 23.

shown. Lardo *et al.*[21] proposed a method to quantify the MR signal changes in cardiac tissue after RF ablation and correlate MR lesion size with histological markers of cell death. In Fig. 7.7, the difference between normal tissue and ablated tissue is shown. Plate XXI (see colour section) shows the direct visualization of the lesion and the image of the lesion that is obtained by MR ten minutes after ablation.

7.2.5 Balloon angioplasty

Development of loopless antenna now allows easy guiding and active tracking of interventional procedures. The ability of a loopless antenna to

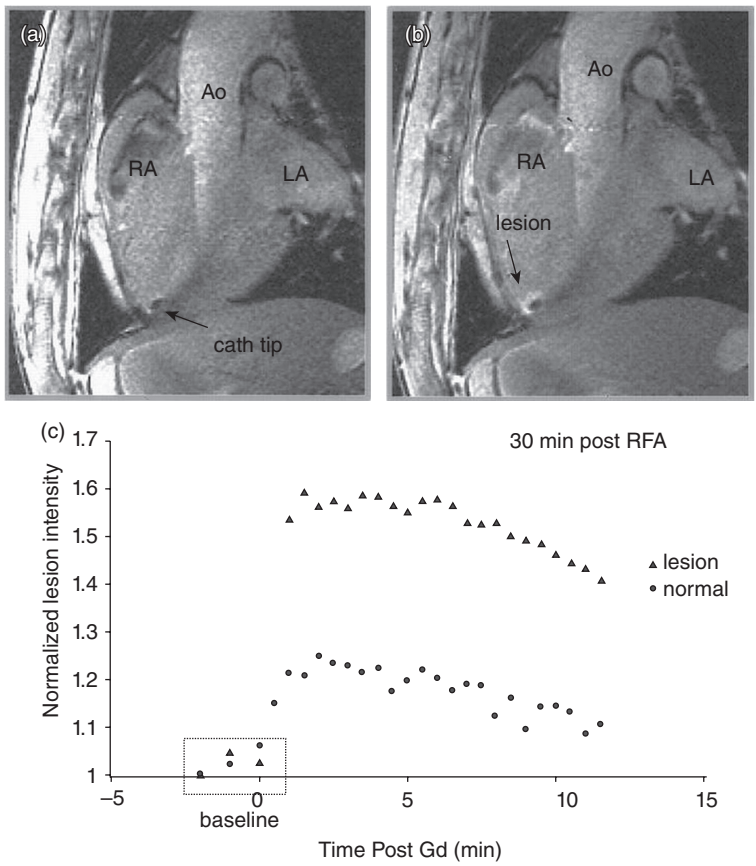

7.7 T1-weighted gradient-echo images (a) before and (b) after 7 mL peripheral gadolinium-DTPA contrast agent with (c) corresponding lesion intensity data showing temporal response for a right ventricular lesion and adjacent segment of normal myocardium. Spatial extent of lesion was clearly demarcated 1 minute after contrast injection. Temporal resolution was 30 seconds. Republished from Reference 21.

obtain high-resolution images of vessel walls can be helpful for balloon angioplasty operations. Using a loopless antenna, stenosis can be located and a balloon catheter can be guided to the desired location to perform the operation. Yang *et al.*[24,25] have successfully demonstrated such balloon angioplasty under MRI. Figure 7.8 demonstrates the artificial stenosis and the balloon angioplasty procedure; Fig. 7.9 features the loopless catheter antenna and balloon catheter used in Reference 24. Due to the artificial stenosis, only a mild contrast enhancement is seen in the kidneys. However, after angioplasty the contrast enhancement quickly increased.[26] A different approach was demonstrated by Quick *et al.*,[26] in which an expandable single loop RF coil was replaced on the balloon itself.

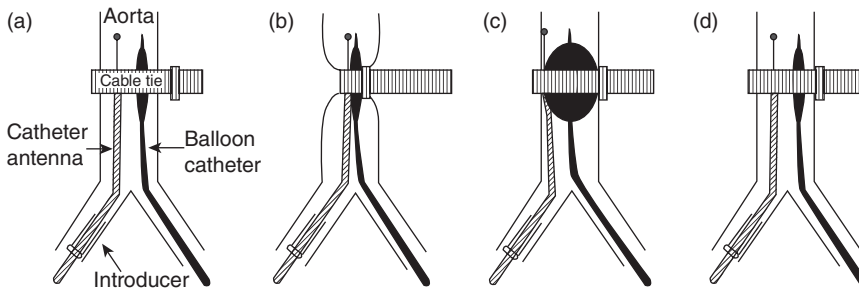

7.8 Illustration of the experimental design for an intravascular MR-monitored balloon angiogplasty on a rabbit. Republished from Reference 24.

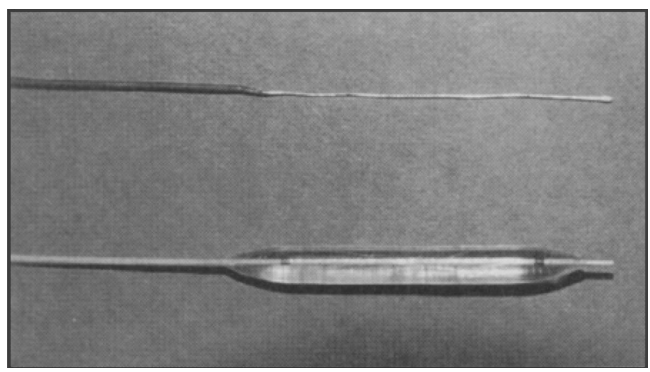

7.9 The tip of the catheter antenna (upper) and the tip of the balloon catheter (lower). Republished from Reference 24.

7.2.6 MR-guided aortic valve replacement

It is desirable to use minimal invasion during surgery to reduce trauma and accelerate the recovery of the patient. However, in valve surgery it is still necessary to arrest and empty the heart[27] for visualization of the surgical field. Real-time MRI techniques can provide an alternative to these operations by providing visuals of the surgical field even while the heart is beating. McVeigh *et al.*[27] have demonstrated a MRI-guided valve replacement and in Plate XXII (see colour section between pages 182 and 183), the valve and carrier catheter are shown. In this work, preparatory imaging was performed in order to determine the orientation of the heart and plan the procedure. Figure 7.10 shows selected frames from the valve replacement operation. Of the eight pigs used in this study, four survived after valve implantation.

7.3 Catheter visualization

MR uses the radio frequency (RF) signal from the tissue; unlike with X-ray fluoroscopy, traditional catheters are not visible in MR images. To visualize catheters in MR images, modifications are required. One solution to this problem is to place RF coils on the catheters, making them capable of picking up or altering the RF fields. Over the past few decades, researchers have designed several ways to make catheter coils visible. Besides their visualization properties, catheter coils have the ability to obtain high-resolution images of the blood vessels. During the design of the catheter coils, it is therefore important that not only are their RF properties taken into account, but also their mechanical properties and dimensions.

The dimension of the catheter coils is an important feature which depends on the intended application. Usually, the maximum diameter of the catheters is measured in units of Fr (French). A 3Fr diameter corresponds to 1 mm or 0.039 inches.[28] Most catheters have more than one lumen for different purposes; some are used for guidewires whilst others may be used for carrying surgical apparatus or injection needles.

A guidewire must have the ability to carry the force from the distal end to the proximal end without damaging the vessels. The distal end of the guidewire should also have the ability to turn so that it can be guided to the desired location. These properties are important for safe, efficient navigation of the guidewire inside the vessels. Other types of catheters, such as balloon catheters for example, are used with the help of guidewires and guiding catheters.

Understanding these mechanical properties is therefore important for the design of the catheter coils, as any coil or electronic circuit that is placed inside a catheter may affect the catheter's mechanical properties.

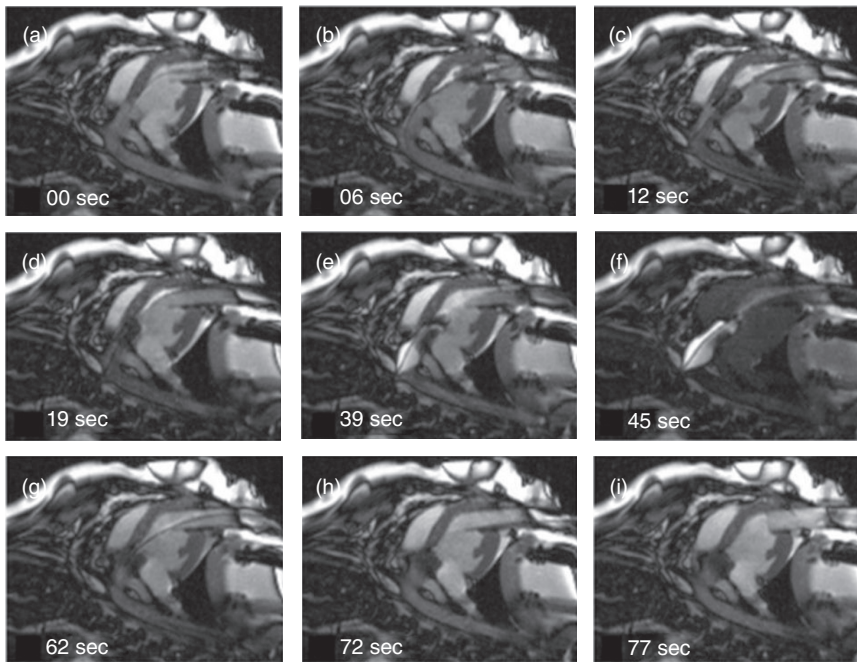

7.10 Selected frames from the real-time MRI displayed within the scan room, showing the deployment of the prosthetic valve. (a) A guidewire is advanced through the trocar across the native aortic valve. (b) The prosthetic valve is advanced to the end of the trocar. (c) The prosthetic valve is advanced into position in the LV outflow track. (d) The prosthetic valve is inserted across the native valve and aligned with the coronary ostia and the aortic annulus. (e) A balloon filled with dilute Gd-DTPA MR contrast agent is used to expand the prosthetic valve. (f) Interactive saturation is used to enhance visualization of the extent of balloon inflation. (g) The balloon is taken down and pulled back through the trocar. (h) The guidewire is removed. (i) The delivery device is removed from the trocar. The total time required for this sequence of pictures was 77 s. (Also see the movie in the National Heart, Lung, and Blood Institute [NHLBI] archive: http://imagegallery.nhlbi.nih.gov/mcveighe/mrm1.html) Republished from Reference 27.

7.3.1 Elongated loop coil design

Loop coils are widely used as surface coils in MRI, so are also good candidate for catheter coils. A loop coil can be formed by using two parallel wires shortened at the distal end. The proximal end can be used as the terminal port of the coil and the signal can be transferred using a coaxial cable. Tuning and decoupling of the coil can be done either at the terminal site[9]

or remotely at the end of the coaxial line.[29] Circuit diagrams of both techniques are shown in Figures 7.11 and 7.12.

A detailed analysis of loop coils and their SNR performance has been conducted by Atalar *et al.*[9] The proposed catheter was 4.5 mm at the tuning part and had a 1.5 mm coil, as shown in Fig. 7.13. The coil was constructed with two parallel wires shortened at the distal end and tuned and matched at the proximal end. For decoupling from the transmit coil, a shunt PIN

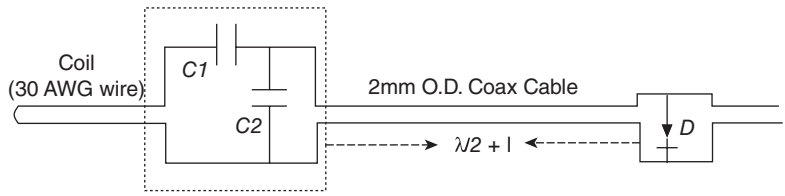

7.11 Circuit diagram of loop catheter coil from Reference 9. Tuning and matching networks and decoupling diode are shown in the figure.

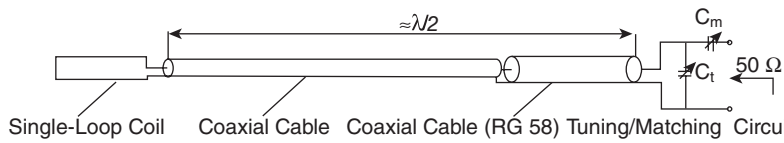

7.12 Schematic of catheter used in Reference 29. The matching and tuning network was placed far from the coil.

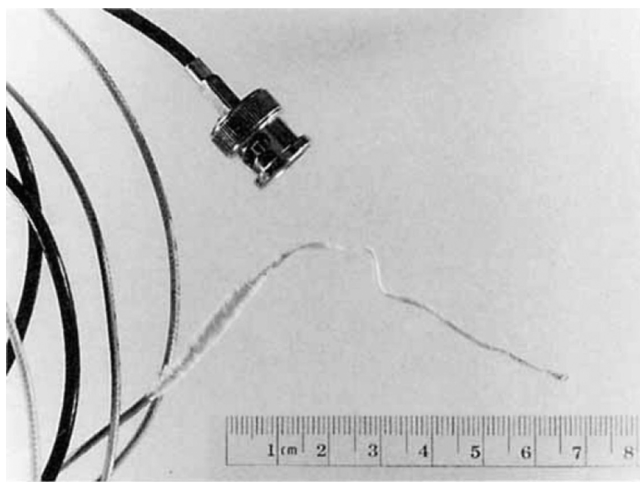

7.13 Picture of the loop coil that is used in Reference 9 (Reproduced from Reference 9).

diode was placed on the coaxial cable and the position of the diode adjusted to minimize the induced currents when the diode was on.

SNR analysis of loop coils has also been well explained by Atalar *et al.*[9] using transmission line theory, by which noise is proportional to the square root of the real part of the impedance measured at the terminal of the coil. Finding signal strength as a function of the position reciprocity principle can also be used. A unit voltage can be applied to the terminal of the loop coil, allowing calculation of the magnetic field at a desired point. Then the ratio of the generated magnetic field to the real part of the measured terminal impedance gives a measurement for SNR. An example SNR map of a loop catheter coil is shown in Fig. 7.14.[9] SNR of the loop coil increases with the wire separation. In addition, the dielectric material has an important role in the SNR of a loop coil as SNR increases with insulation thickness. This is exhibited particularly well by low losses from insulation around the tuning capacitor. The resistive loss of the wire is also important as for short coils the dominant noise source is the wire resistance.

When the coil is oriented with the main magnetic field (B0), it has a uniform sensitivity along the circumferential direction. However, when the orientation of the coil varies from the main magnetic field, circumferential nonuniformity can be observed. Loop coils' sensitivities also drop with any increase in distance from the coil. It is difficult to see all the desired parts of the image with a single brightness and contrast adjustment; when brightness and contrast are adjusted to see around the coil, anything far outside the approximate radius of the coil will not be visible, while if the contrast and brightness are adjusted to see areas far away from the coil,

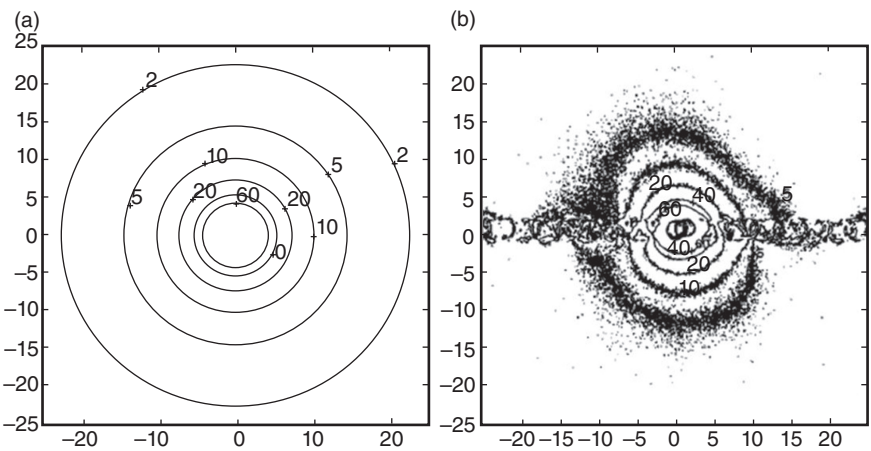

7.14 The sensitivity map of the catheter coil. (a) Theoretical calculations. (b) Experimental results with TR 6000 and TE 34 ms. (Reproduced from Reference 9.)

places around the coil will be saturated in the image. One solution to this is to calculate the sensitivity map and multiply the image with the inverse of this map. However, both the coil position and the orientation must be known, as the sensitivity map will be different for every orientation of the coil. In addition, increasing the distance of the coil's wire separation allows desired parts of the image to be seen once, but the size of the catheter limits the wire separation, meaning this technique is not ideal. One solution to overcome this problem has been proposed by Quick *et al.*[29] in the form of an expandable coil. The coil is mounted on the inflatable balloon, as shown in Fig. 7.15, and in its deflated state the catheter can be easily maneuvered through the vessels. However, the shape of the coil may not be reproduced, so the matching and tuning may spoil. This problem has been addressed by Quick *et al.* by constructing the coil using elastic material. If the coil is to be used for tracking of the catheter rather than imaging, the twisted loop is a good candidate.[30] A twisted loop can be as thin as a guidewire and, as the sensitivity drops dramatically with distance from the coil field of view (FOV), this coil is extremely small, allowing researchers to detect coil position accurately.

When constructing a loop coil, fixed value surface mount capacitors are used due to their small size. This capacitance can be put at the terminal of

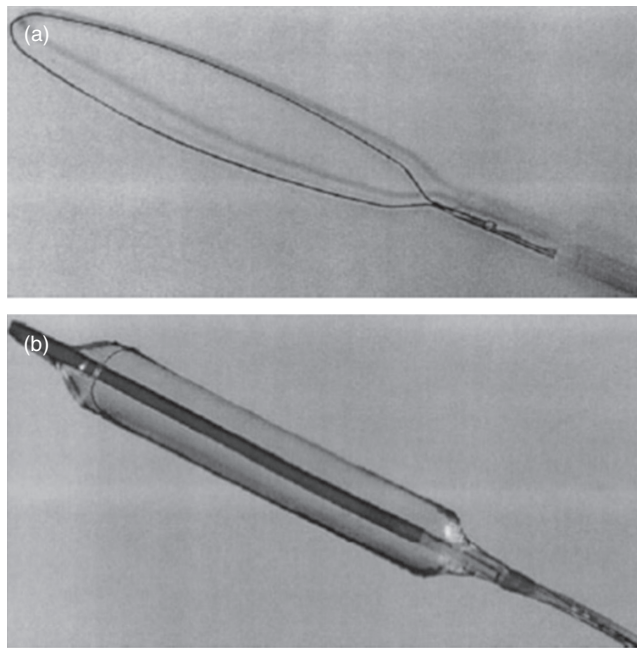

7.15 Catheter prototypes from Reference 29. (a) NiTinol single loop coil. (b) Balloon mounted single-loop copper coil.

the loop or can be distributed along it. Distributed capacitance decreases the load-dependence of the resonance frequency. It also improves the SNR performance of the coil, but as the main loss factor is the wire resistance, SNR improvement will be limited. The length of the coil can also be adjusted for a given capacitance. As the tuning and matching capacitors can be placed on the terminal site, they can also be placed at the end of the coaxial cable, although this will produce an SNR drop. When tuning and matching a loop coil, unbalanced currents must be taken into account, as in the matching and tuning networks the electrical balance must be maintained. In the case of a failure, SNR can significantly drop and unsymmetrical SNR maps will be obtained. The inductance changes caused by flexing inside the tissue must also be considered, as the change in inductance will cause shifts in the resonance frequency and SNR drops. However, this problem has been addressed by using electronic tuning with varactor diodes,[31] although varactor diodes are another source of noise and can further cause SNR degradation.

At the end loop, catheter coils have been well studied and are well understood. The parameters that affect their performance are well documented and can be optimized by considering the electrical performance and the mechanical properties.

7.3.2 Loopless antenna design

The loopless antenna was first proposed by Ocali and Atalar[10] and is a coaxial cable with an extended inner conductor, as shown in Fig. 7.16. As the loopless antenna does not have any capacitors, the thickness of the catheter is limited by the thickness of the coaxial cable. However, while choosing a coaxial cable, mechanical constraints must be taken into

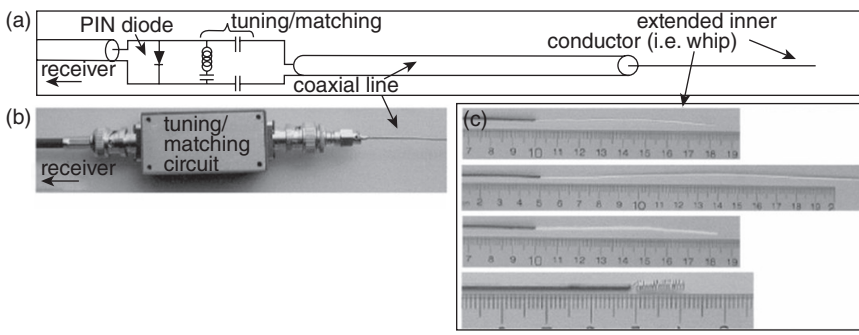

7.16 Basic design of loopless antenna. (a) The schematic of loopless antenna. (b) Matching and tuning networks. (c) Antenna whip. (Reproduced from Reference 33.)

account. In Reference 32, for example, materials that are used for internal MRI antennas are explored and use of a 0.014 in. loopless antenna as a guidewire is demonstrated.

The SNR of a loopless antenna is optimized by adjusting the whip (extended inner conductor) length.[10] For a bare wire, the optimum whip length is approximately $\lambda/4$ at the operating frequency inside the body. For 1.5T, $\lambda/4$ corresponds to nearly 10 cm. This length can be decreased by coiling the whip.[33] Susil *et al.* have also shown that by insulating the whip, the optimum length can be increased. The loopless antenna is similar to the loop antenna in that it has uniform sensitivity along the circumferential direction. The sensitivity of the loopless antenna drops with the inverse of the distance from the catheter, meaning it performs more effectively than the loop antenna in the radial direction. However, unlike loop coils, the sensitivity of the loopless antenna varies significantly. At the connection point of the whip and the coaxial cable, SNR reaches the maximum point, and drops towards the end of the whip, reaching approximately zero. However, this problem has been addressed by Qian *et al.*[34] by tapering the whip. Sensitivity maps of the traditional loopless antenna and tapered whipped loopless antenna are shown in Fig. 7.17. Another solution for the SNR variation was proposed by Serfaty *et al.*[35] which involved connecting a solenoid, which has increasing pitch toward the tip, to the whip. A further loopless antenna design was also demonstrated by Erturk *et al.*[36] at 7T field strength.

Decoupling of a loopless antenna is rather easy. A shunt PIN diode placed $\lambda/4$ away from the junction point will solve the problem of coupling to the transmit coil. To address safety concerns, a designer may integrate a series DC block capacitor to prevent the flow of the DC current to the body. Similarly, a designer may want to eliminate induced shield currents, although the decoupling network partially handles this problem. However, as the shield is a part of the antenna during reception, induced shield currents are required for imaging, so as an alternative, a balun circuit can be constructed near the external decoupling network. An additional RF shield in the form of bazooka balun can also be used, but this may affect the flexibility and SNR of the coil.

7.3.3 Solenoid coil design

Solenoid coils are an alternative to loop coils and loopless antenna.[37,38] A very short solenoid is usually used for determining the position of the catheter. When these coils are used for tracking of the catheter, SNR uniformity around the coil is not a serious problem so no tuning and matching capacitances are used and the signal is carried directly with a twisted pair or a coaxial cable. The use of decoupling diodes is also absent

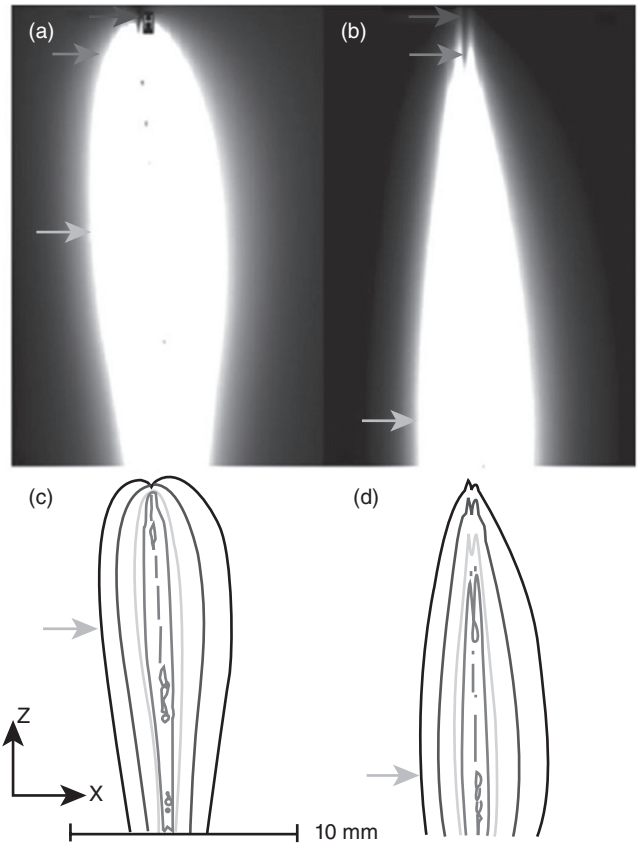

7.17 Sagittal Images from the phantom. (a) The tapered-insulation loopless antenna. (b) Uniform insulation loopless antenna. (c) and (d) are the SNR maps of the tapered-insulation and uniform insulation loopless antennas, respectively. (Reproduced from Reference 34.)

from use with these coils. Multiple solenoids can be placed on a catheter in order to visualize various parts.

As well as tracking, solenoid coils can also be used for imaging purposes. However, in this case tuning, matching and decoupling of the coil become important, as when using loop coils. The use of opposed solenoids has been proposed for imaging purposes. An opposed solenoid is formed by placing apart two solenoids with opposite pitching directions. Opposed solenoids create fairly uniform SNR maps around the coil[39–41] including across the gap between them. However, this uniformity does come with an additional loss in SNR. Hurst *et al.*[42] addressed this by placing a field effect transistor inside the catheter to overcome the SNR loss. Alternatively, another solenoid coil design features orthogonal solenoid coils.[43] In this design, two orthogonal

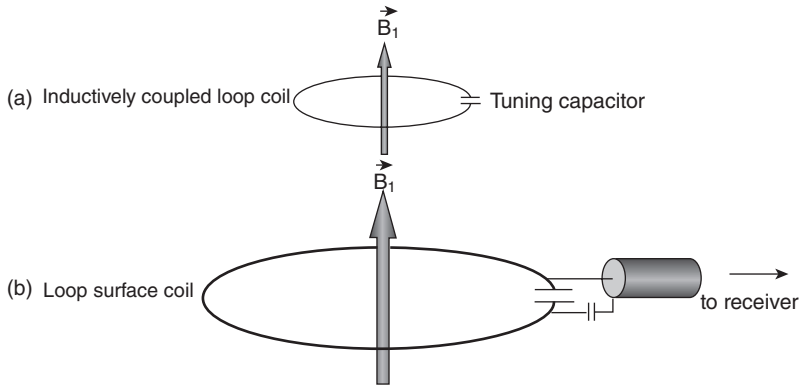

7.18 Inductively coupled coil design. Coupling between (a) surface coil and (b) catheter-mounted inductively coupled coil is described. (Reproduced from Reference 16.)

solenoid coils were placed and oriented by 45 degrees with respect to the axis of the catheter. With this design, a fairly uniform SNR map was obtained around the coil, including at the front of the catheter.

7.3.4 Inductively coupled radio frequency (RF) coils

The major difference between inductively coupled RF (ICRF) coils and other coils is that there is no need for a connection from the ICRF coils to the scanner. An ICRF coil is usually a tuned loop coil. When imaging is done with a standard surface body coil, there will be an amplified signal around the ICRF coil.[16] The working principle behind the ICRF coil is shown in Fig. 7.18. When a current is applied to the transmit coil, there will be a high induced current on the tuned ICRF coil. The induced currents will generate a magnetic field in the vicinity of the ICRF coil and the signal around the ICRF coil will be amplified. However, in some cases, high induced currents can be harmful to the patient and can cause image artifacts. To solve these problems, back-to-back Shottky diodes can be connected to the coil.[44]

7.4 Tracking using intravascular MR coils

One of the main purposes of placing coils on catheters is tracking catheter position and orientation. Tracking techniques can generally be characterized as either active catheter tracking or passive catheter tracking. In passive catheter tracking, a marker is usually placed on the catheter in order to create an artifact in the image. This technique can easily be implemented by using solenoid coils. The main problem in using this technique is finding

the position of the artifact during the vascular operation. If the artifact is large it can spoil the image, but if the artifact is small then it is easy to lose the position of the catheter. Another method to implement passive catheter tracking is the use of reverse polarization with ICRF coils, as proposed by Celik *et al.*[44,45] Celik proposed the use of forward and reverse polarized images obtained via multiple coils, to gain information on both the body and the position of the catheter. Active catheter tracking is an alternative to passive tracking methods. Although it solves the visibility problem, there is an associated increase in the complexity of the design and RF safety problems. In active catheter tracking methods, the catheter coil is directly connected to the scanner. Loopless antennas are a good choice for tracking due to their shaft visibility properties, and using a loopless antenna, guidewires can be visualized under MRI. The loopless design has been successfully used as a needle antenna[46,47] as shown in Fig. 7.19, whilst injection catheters using the loopless design have also been manufactured,[48,49] and the design further used for the tracking of guidewires in balloon angioplasty procedures.[50]

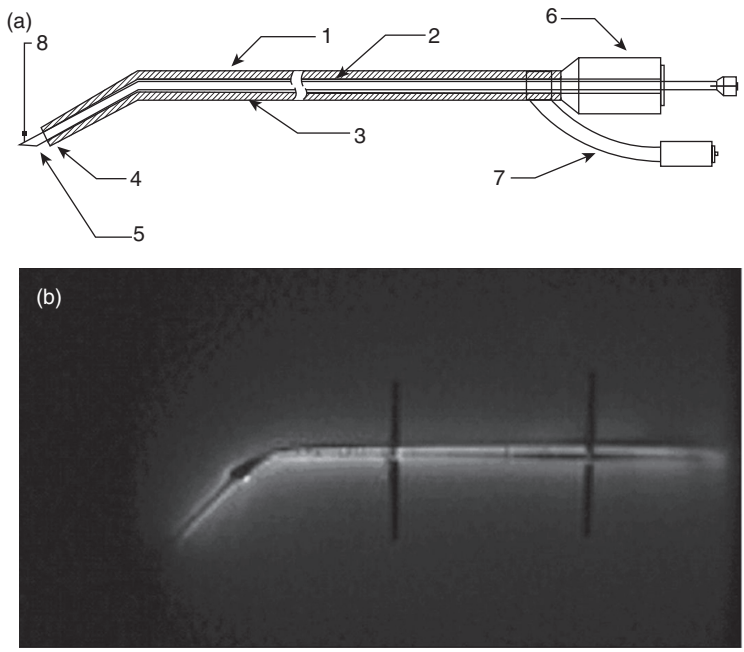

7.19 Loopless design as puncture needle. 1. Outer nitinol tube. 2. Inner nitinol tube with a polyimide liner. 3. Nylon dielectric. 4. Copper wire coil. 5. Three-face bevel. 6. Connector for syringe. 7. Coaxial cable connector to interface circuit. 8. Removable nitinol puncture needle. Reproduced from Reference 46.

7.5 Signal-to-noise ratio (SNR) performance of catheter coils

The variety of catheter coils available, all of which feature their own specific advantages and disadvantages, may make choosing the appropriate one for a particular application difficult. It is hard to compare catheter coils without knowing the exact conditions of their intended application. For example, in areas with small dimensions, use of a loopless coil gives better SNR than use of a loop coil, whilst in areas with larger dimensions, loop coils are more efficient. However, comparing coils with each other can be difficult and also increases the possibility of missing particularly important cases. As such, there is a need for a quantity which is a measure of coil SNR performance, and ultimate intrinsic signal-to-noise ratio was defined by Ocali and Atalar[6] as just such a measure for performance analysis of surface coils. It is well known that the MRI signal depends on the transverse component of the magnetic field generated by the RF coil, and the main noise source is the body. This is related to the electric field, which is generated by the same RF coil under the same conditions. To achieve the ultimate value of SNR, noise generated, aside from that produced by the body, must be zero. To find the maximum SNR, the magnetic field must be maximized and the electric field must be minimized. In Ocali and Atalar's work, the optimization problem was solved without imposing restrictions on the coil design, instead considering only the electromagnetic fields inside the body and finding the optimum field for the ultimate intrinsic SNR value numerically. They then compared various coil designs with the ultimate value of the intrinsic SNR. This study was extended by Kopanoglu *et al.*[7] to find an analytical expression for the Ultimate Intrinsic SNR. The UISNR formulation shows that SNR reaches infinity at the surface of the body and decreases with the 2.5th power of the distance, meaning that for higher SNR values internal coils are necessary. Ultimate intrinsic SNR analysis of internal coils was also conducted by Celik *et al.*[8] Figure 7.20 shows that a loopless antenna performs better than the body coil for the points of interest, which are close to the center of the body. It should be noted that the loopless antenna is not the best internal coil in terms of SNR performance.

7.6 Safety of intravascular catheters

As previously noted, catheter coils are key to tracking catheters or obtaining high resolution images of the vascular system. As these coils are tuned to the Larmor Frequency, they will have strong coupling with the transmitted RF field if no precautions are taken against this. The coupled RF field will cause heating and in some cases tissue burn, so it is important that the RF safety of a catheter coil is verified before use.

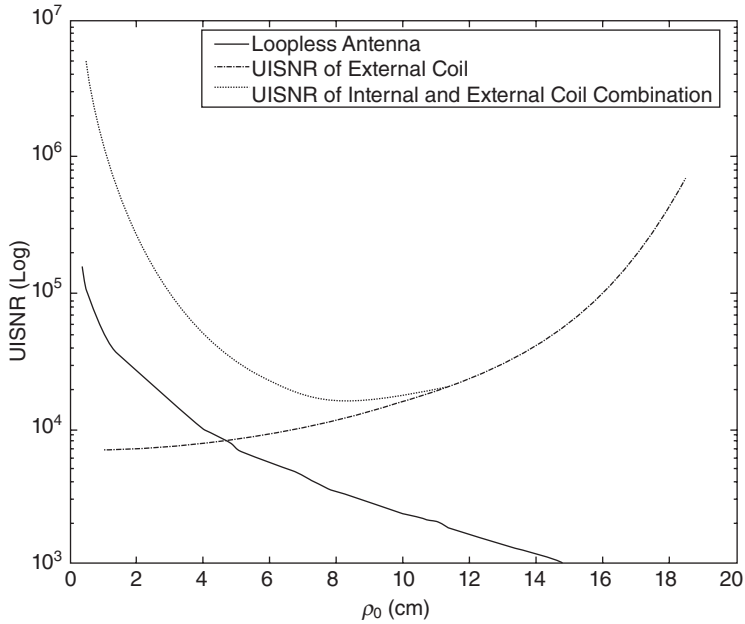

7.20 A comparison of three ISNR values. ρ_0 is the radial distance of the point of interest from the center of the object. The internal coil is effective at points near the cavity, and then the external coil becomes effective as the point of interest approaches the outer boundary on the curve of the UISNR of an internal and external coil combination. In this figure, the external coil has a 20 cm body radius, and the internal and external coil combination has a 20 cm body radius and a 0.375 mm cavity radius. The radius of the loopless antenna is 0.375 mm. Reproduced from Reference 8.

Although the RF safety of catheters can be established using decoupling networks and baluns,[33] they have to be tested to ensure RF safety. At RF frequencies, magnetic fields have a heating effect. For the analysis of this heating phenomena, specific absorption rate (SAR) has been defined as a measure of deposited RF power. For patients without implants or catheters, MRI can be conducted within safe RF limits. However, in the presence of a metallic catheter, SAR will be amplified at the tip of the catheter. This SAR amplification can be defined with SAR gain as follows;

$$\mathrm{SAR}_{\mathrm{gain}} = \frac{\mathrm{SAR}_{\mathrm{implant}}}{\mathrm{SAR}_{\mathrm{incident}}} \qquad [7.1]$$

This SAR gain can be related to RF heating via bioheat transfer.[51] When the SAR gain is known, the temperature increase can be calculated by convolution with the appropriate Greens function. SAR gain is not,

therefore, enough for analysis of temperature increase around a catheter tip, as it does not contain the effect of bioheat transfer. To address this, the Safety Index was defined by Yeung *et al.*,[51] taking the effect of bioheat transfer into account. The Safety Index estimates the *in vivo* temperature increase at the tip of a wire for applied SAR, making it useful for setting limits to SAR and also for investigating the RF safety of catheters.

There are also different test methods for RF safety tests of catheters. Graesslin *et al.*[52] proposed that by monitoring the currents in RF transmit elements, unsafe conditions can be determined during an interventional procedure. In addition, Etezadi-Amoli *et al.*[53] have shown that by monitoring the induced currents on a catheter, a decoupled RF excitation can be found.

Gradient fields must also be investigated, as gradient-induced currents along the catheters may cause nerve stimulation. Turk *et al.* analytically investigated the gradient safety of implants in their work.[54] The issue of gradient-induced currents has been solved for any gradient coil due to the fact that the catheter is in the linear region of the gradient coil; using Turk's work, the electrical potential at the catheter tip can be calculated for any known gradient and catheter position, allowing the risk of nerve stimulation to be predicted.

Another important concern is related to the mechanical safety of the catheter. Replacing a coil inside a catheter requires compromising the catheter's mechanical properties, so mechanical tests must be performed in order to ensure that the catheter will function properly during the interventional procedure.

7.7 Conclusion

The discussion of key intravascular interventions and catheters, along with the intravascular diseases and MR principles explored in this chapter, provides a general overview of the use of MR in intravascular operations. Developments in catheter coil designs and their SNR performances, along with advances in safety analysis of the catheter coils, reveal the range of techniques currently achievable using this technology and hint at even more beneficial developments in the future. Designs are continually developing, and it is suggested that the reader explores the detailed analysis of these topics as contained in the referenced original articles. However, the information given in this chapter should provide a good basic grounding in the key principles required for the understanding of intravascular MRI catheters.

7.8 References

1 D. Tomazevic, B. Likar, T. Slivnik and F. Pernus. 3-D/2-D Registration of CT and MR to X-Ray images, *IEEE Transactions on Medical Imaging*, 2003;22(11).

2 J. L. Boxerman, T. J. Mosher, E. R. McVeigh, E. Atalar, J. A. Lima and D. A. Bluemke. Advanced MR imaging techniques for evaluation of the heart and great vessels, *Radiographics*, 1998;18:543–564.
3 C. Yuan, W. S. Kerwin, M. S. Ferguson, N. Polissar, S. Zhang, J. Cai and T. S. Hatsukami. Contrast-enhanced high resolution MRI for atherosclerotic carotid artery tissue characterization, *Journal of Magnetic Resonance Imaging*, 2002; 15:62–67.
4 Z. A. Fayad, V. Fuster, K. Nikolaou, *et al.* Computed tomogramphy and magnetic resonance imaging for noninvasive coronary angiography and plaque imaging: current and potential future concepts, *Circulation*, 2002;106:2026–2034.
5 M. Stuber, R. M. Botnar, K. V. Kissinger, W. J. Manning. Free-breathing black-blood coronary MR angiography: initial results, *Radiology*, 2001;219(1): 278–283.
6 O. Ocali and E. Atalar. Ultimate intrinsic signal-to-noise ratio, *MRI in Magnetic Resonance Medicine*, 1998;39:462–473.
7 E. Kopanoglu, V. B. Erturk and E. Atalar. Analytic expressions for the ultimate intrinsic signal-to-noise ratio and ultimate intrinsic specific absorption rate in MRI, *Magnetic Resonance in Medicine*, 2011;66:846–858.
8 H. Celik, Y. Eryaman, A. Altintas, I. A. Abdel-Hafez and E. Atalar. Evaluation of internal MRI coils using ultimate intrinsic SNR, *Magnetic Resonance in Medicine*, 2004;52:640–649.
9 E. Atalar, P. A. Bottomley, O. Ocali, L. C. Correia, M. D. Kelemen, J. A. Lima and E. A. Zerhouni. High resolution intravascular MRI and MRS by using a catheter receiver coil, *Magnetic Resonance in Medicine*, 1996;36: 596–605.
10 O. Ocali and E. Atalar. Intravascular magnetic resonance imaging using a loopless catheter antenna, *Magnetic Resonance in Medicine*, 1997;37: 112–118.
11 L. C. Correia, E. Atalar, M. D. Kelemen, O. Ocali, G. M. Hutchins, J. L. Fleg, G. Gerstenblith, E. A. Zerhouni and J. A. Lima. Intravascular magnetic resonance imaging of aortic atherosclerotic plaque composition, *Arteriosclerosis, Thrombosis and Vascular Biology*, 1997;17:3626–3632.
12 W. J. Rogers, J. W. Prichard, Y. L. Hu, P. R. Olson, D. H. Benckart, C. M. Kramer, D. A. Vido and N. Reichek. Characterization of signal properties in atherosclerotic plaque components by intravascular MRI, *Arteriosclerosis, Thrombosis and Vascular Biology*, 2000;20:1824–1830.
13 G. G. Zimmermann-Paul, H. H. Quick, P. Vogt, G. K. von Schulthess, D. Kling and J. F. Debatin. High-resolution intravascular magnetic resonance imaging: monitoring of plaque formation in heritable hyperlipidemic rabbits, *Circulation*, 1999;99:1054–1061.
14 L. V. Hofmann, R. P. Liddell, J. Eng, *et al.* Human peripheral arteries: feasibility of transvenous intravascular MR imaging of the arterial wall, *Radiology*, 2005;235(2):617–622.
15 R. M. Botnar, A. Bücker, W. Y. Kim, I. Viohl, R. W. Günther and E. Spuentrup. Initial experiences with *in vivo* intravascular coronary vessel wall imaging, *Journal of Magnetic Resonance Imaging*, 2003;17:615–619.
16 H. H. Quick, H. Kuehl, G. Kaiser, S. Bosk, J. F. Debatin and M. E. Ladd. Inductively coupled stent antennas in MRI, *Magnetic Resonance in Medicine*, 2002;48: 781–790.

17 E. Spuentrup, A. Ruebben, T. Schaeffter, W. J. Manning, R. W. Gunther and A. Buecker. Magnetic resonance-guided coronary artery stent placement in a swine model, *Circulation*, 2002;105:874–879.
18 A. N. Raval, P. V. Karmarkar, M. A. Guttman, C. Ozturk, S. Sampath, R. DeSilva, R. J. Aviles, M. Xu, V. J. Wright, W. H. Schenke, O. Kocaturk, A. J. Dick, V. K. Raman, E. Atalar, E. R. McVeigh and R. J. Lederman. Real-time magnetic resonance imaging-guided endovascular recanalization of chronic total arterial occlusion in a swine model, *Circulation*, 2006;113:1101–1107.
19 *ACC/AHA/ESC 2006 Guidelines for the Management of Patients with Atrial Fibrillation*: a report of the American College of Cardiology/American Heart Association Task Force on Practice Guidelines and the European Society of Cardiology Committee for Practice Guidelines (Writing Committee to Revise the 2001 Guidelines for the Management of Patients with Atrial Fibrillation): developed in collaboration with the European Heart Rhythm Association and the Heart Rhythm Society, *Circulation*, 2006;114(7):e257–354.
20 R. C. Susil, C. J. Yeung, H. R. Halperin, A. C. Lardo and E. Atalar. Multifunctional interventional devices for MRI: a combined electrophysiology/MRI catheter, *Magnetic Resonance in Medicine*, 2002;47:594–600.
21 A. C. Lardo, E. R. McVeigh, P. Jumrussirikul, R. D. Berger, H. Calkins, J. Lima and H. R. Halperin. Visualization and temporal/spatial characterization of cardiac radiofrequency ablation lesions using magnetic resonance imaging, *Circulation*, 2000;102:698–705.
22 S. Nazarian, A. Kolandaivelu, M. M. Zviman, G. R. Meininger, R. Kato, R. C. Susil *et al.* Feasibility of real-time magnetic resonance imaging for catheter guidance in electrophysiology studies, *Circulation*, 2008;118:223–229. [Epub 2008 Jun 23]
23 T. Dickfeld, R. Kato, M. Zviman *et al.* Characterization of radiofrequency ablation lesions with gadolinium-enhanced cardiovascular magnetic resonance imaging, *Journal of the American College of Cardiology*, 2006;47(2):370–378.
24 X. Yang, B. D. Bolster, D. L. Kraitchman and E. Atalar. Intravascular MR-monitored balloon angioplasty: an *in vivo* feasibility study, *Journal of Vascular and Interventional Radiology*, 1998;9:953–959.
25 X. Yang and E. Atalar. Intravascular MR imaging-guided balloon angioplasty with an MR imaging guide wire: feasibility study in rabbits, *Radiology*, 2000;217:501–506.
26 H. H. Quick, M. E. Ladd, P. R. Hilfiker, G. G. Paul, S.-W. Ha and J. F. Debatin. Autoperfused balloon catheter for intravascular MR imaging, *Journal of Magnetic Resonance Imaging*, 1999;9:428–434.
27 E. R. McVeigh, M. A. Guttman, R. J. Lederman, M. Li, O. Kocaturk, T. Hunt, S. Kozlov and K. A. Horvath. Real-time interactive MRI-guided cardiac surgery: aortic valve replacement using a direct apical approach, *Magnetic Resonance in Medicine*, 2006;56:958–964.
28 http://en.wikipedia.org/wiki/French_catheter_scale, *French catheter scale*, July 2011, accessed 15/12/2012.
29 H. H. Quick, M. E. Ladd, G. G. Zimmermann-Paul, P. Erhart, E. Hofmann, G. K. von Schulthess and J. F. Debatin. Single-loop coil concepts for intravascular magnetic resonance imaging, *Magnetic Resonance in Medicine*, 1999;41: 751–758.

30 M. Burl, G. A. Coutts, D. J. Herlihy, R. Hill-Cottingham, J. F. Eastham, J. V. Hajnal and I. R. Young. Twisted-pair RF coil suitable for locating the track of a catheter, *Magnetic Resonance in Medicine*, 1999;41:636–638.
31 K. Kandarpa, P. Jakab, S. Patz, F. J. Schoen and F. A. Jolesz. Prototype miniature endoluminal MR imaging catheter, *Journal of Vascular and Interventional Radiology*, 1993;4:419–427.
32 B. Qiu, P. Karmarkar, C. Brushett, F. Gao, R. Kon, S. Kar, E. Atalar and X. Yang. Development of a 0.014-inch magnetic resonance imaging guidewire, *Magnetic Resonance in Medicine*, 2005;53:986–990.
33 R. C. Susil, C. J. Yeung and E. Atalar. Intravascular extended sensitivity (IVES) MRI antennas, *Magnetic Resonance in Medicine*, 2003;50:383–390.
34 D. Qian, A.-M. M. El-Sharkawy, E. Atalar and P. A. Bottomley. Interventional MRI: tapering improves the distal sensitivity of the loopless antenna, *Magnetic Resonance in Medicine*, 2010;63:797–802.
35 J. M. Serfaty, X. Yang, P. Aksit, H. H. Quick, M. Solaiyappan and E. Atalar. Toward MRI-guided coronary catheterization: visualization of guiding catheters, guidewires, and anatomy in real time, *Journal of Magnetic Resonance Imaging*, 2000;12:590–594.
36 M. A. Ertürk, A.-M. M. El-Sharkawy and P. A. Bottomley. Interventional loopless antenna at 7T, *Magnetic Resonance in Medicine*, 2012;68:980–988.
37 J. Ackerman, M. Offutt, R. Buxton and T. Brady. Rapid 3D tracking of small RF coils, *Proceedings of the 5th Annual Metting of SMRM*, Montreal, Quebec, 1986;1131–1132.
38 C. L. Dumoulin, S. P. Souza and R. D. Darrow. Real-time position monitoring of invasive devices using magnetic resonance, *Magnetic Resonance in Medicine*, 1993;29:411–415.
39 A. J. Martin, D. B. Plewes and R. M. Henkelman. MR imaging of blood vessels with an intravascular coil, *Journal of Magnetic Resonance Imaging*, 1992;2: 421–429.
40 A. J. Martin, A. I. Gotlieb and R. M. Henkelman. High-resolution MR imaging of human arteries, *Journal of Magnetic Resonance Imaging*, 1995;5:93–100.
41 A. J. Martin and R. M. Henkelman. Intravascular MR imaging in a porcine animal model, *Magnetic Resonance in Medicine*, 1994;32:224–229.
42 G. C. Hurst, J. Hua, J. L. Duerk and A. M. Cohen. Intravascular (catheter) NMR receiver probe: preliminary design analysis and application to canine iliofemoral imaging, *Magnetic Resonance in Medicine*, 1992;24:343–357.
43 K. J. T. Anderson, G. Leung, A. J. Dick and G. A. Wright. Forward-looking intravascular orthogonal-solenoid coil for imaging and guidance in occlusive arterial disease, *Magnetic Resonance in Medicine*, 2008;60:489–495.
44 H. Celik and E. Atalar. Reverse polarized inductive coupling to transmit and receive radiofrequency coil arrays, *Magnetic Resonance in Medicine*, 2012;67:446–456.
45 H. Celik, A. Ulutürk, T. Tali and E. Atalar. A catheter tracking method using reverse polarization for MR-guided interventions, *Magnetic Resonance in Medicine*, 2007;58:1224–1231.
46 A. Arepally, P. V. Karmarkar, C. Weiss, E. R. Rodriguez, R. J. Lederman and E. Atalar. Magnetic resonance image-guided trans-septal puncture in a swine heart, *Journal of Magnetic Resonance Imaging*, 2005;21:463–467.

47 A. N. Raval, P. V. Karmarkar, M. A. Guttman, C. Ozturk, S. Sampath, R. DeSilva, R. J. Aviles, M. Xu, V. J. Wright, W. H. Schenke, O. Kocaturk, A. J. Dick, V. K. Raman, E. Atalar, E. R. McVeigh and R. J. Lederman. Real-time magnetic resonance imaging-guided endovascular recanalization of chronic total arterial occlusion in a swine model, *Circulation*, 2006;113:1101–1107.
48 A. Arepally, P. V. Karmarkar, C. Weiss and E. Atalar. Percutaneous MR imaging-guided transvascular access of mesenteric venous system: study in swine model, *Radiology*, 2006;238:113–118.
49 P. V. Karmarkar, D. L. Kraitchman, I. Izbudak, L. V. Hofmann, L. C. Amado, D. Fritzges, R. Young, M. Pittenger, J. W. Bulte and E. Atalar. MR-trackable intramyocardial injection catheter, *Magnetic Resonance in Medicine*, 2004;51: 1163–1172.
50 J. M. Serfaty, X. Yang, T. K. Foo, A. Kumar, A. Derbyshire and E. Atalar. MRI-guided coronary catheterization and PTCA: A feasibility study on a dog model, *Magnetic Resonance in Medicine*, 2003;49:258–263.
51 C. J. Yeung, R. C. Susil and E. Atalar. RF safety of wires in interventional MRI: using a safety index, *Magnetic Resonance in Medicine*, 2002;47:187–193.
52 I. Graesslin, S. Krueger, P. Vernickel, J. Achtzehn, K. Nehrke and S. Weiss. Detection of RF unsafe devices using a parallel transmission MR system, DOI: 10.1002/mrm.24558.
53 M. Etezadi-Amoli, P. Stang, A. Kerr, J. Pauly and G. Scott. Parallel transmit with integrated toroidal transceive device visualization, *Proceedings of the International Society of Magnetic Resonance in Medicine*, 2012;20.
54 E. A. Turk, E. Kopanoglu, S. Guney, K. E. Bugdayci, Y. ZiyaIder, V. B. Erturk and E. Atalar. A simple analytical expression for the gradient induced potential on active implants during MRI, *IEEE Transactions on Biomedical Engineering*, 2012;59:2845–2851.